Multiparticle emission in the decay of ^{31}Ar

G. T. Koldste,[1] B. Blank,[2] M. J. G. Borge,[3] J. A. Briz,[3] M. Carmona-Gallardo,[3] L. M. Fraile,[4] H. O. U. Fynbo,[1] J. Giovinazzo,[2] B. D. Grann,[1] J. G. Johansen,[1,*] A. Jokinen,[5] B. Jonson,[6] T. Kurturkian-Nieto,[2] J. H. Kusk,[1] T. Nilsson,[6] A. Perea,[3] V. Pesudo,[3] E. Picado,[4,7] K. Riisager,[1] A. Saastamoinen,[5,†] O. Tengblad,[3] J.-C. Thomas,[8] and J. Van de Walle[9]

[1]*Department of Physics and Astronomy, Aarhus University, DK-8000 Aarhus C, Denmark*
[2]*Centre d'Études Nucléaire de Bordeaux-Gradignan, CNRS/IN2P3-Université Bordeaux I, F-33175 Gradignan Cedex, France*
[3]*Instituto de Estructura de la Materia, CSIC, E-28006 Madrid, Spain*
[4]*Grupo de Física Nuclear, Universidad Complutense, E-28040 Madrid, Spain*
[5]*Department of Physics, University of Jyväskylä, FIN-40351 Jyväskylä, Finland*
[6]*Fundamental Fysik, Chalmers Tekniska Högskola, S-41296 Göteborg, Sweden*
[7]*Sección de Radiaciones, Universidad Nacional, Heredia, Costa Rica*
[8]*GANIL, CEA/DSM-CNRS/IN2P3, F-14076 Caen Cedex 5, France*
[9]*CERN, CH-1211 Geneva 23, Switzerland*

(Received 20 February 2014; published 25 June 2014)

A multihit capacity setup was used to study the decay of the dripline nucleus ^{31}Ar, produced at the ISOLDE facility at CERN. A spectroscopic analysis of the β-delayed three-proton decay of ^{31}Ar is presented for the first time together with a quantitative analysis of the β-delayed $2p\gamma$ decay. A new method for determination of the spin of low-lying levels in the βp daughter ^{30}S using proton-proton angular correlations is presented and used to determine that the spin of the 5.2-MeV level is most likely 3^+ with 4^+ also possible. The half-life of ^{31}Ar is found to be 15.1(3) ms. An improved analysis of the Fermi β strength including the $\beta 3p$-decay mode gives a total measured branching ratio of 3.60(44)%, which is lower than the theoretical value found to be 4.24(43)%. Finally, a previously unidentified γ transition from the isobaric analog state in the decay of ^{33}Ar has been found.

DOI: 10.1103/PhysRevC.89.064315 PACS number(s): 23.40.Hc, 27.30.+t

I. INTRODUCTION

Because dripline nuclei have large β-decay Q values and populate daughter nuclei with low particle-separation energies, their decays are characterized by having many open channels [1]. This implies that decays at the dripline provide unique possibilities to study exotic decay modes such as two- and even three-proton emission. The many decay channels unfortunately also complicate the extraction of the decay strength. Here we show that by using a multihit detection setup it is possible to both map the β strength and study the exotic decay modes for the dripline nucleus ^{31}Ar.

The proton-rich argon isotopes can be produced with relative high yields and low contamination from CaO targets using the Isotope Separation On-Line (ISOL) technique, which makes ^{31}Ar an ideal nucleus to choose for this type of study. A schematic decay scheme of ^{31}Ar is shown in Fig. 1. During the past decades the decay of this isotope has been studied in several experiments at the ISOLDE radioactive ion beam facility at the European research organization CERN. The first interest in this nucleus arose from the possibility of detecting ground state two-proton ($2p$) decay, but this decay mode has not yet been identified in this decay. However, ^{31}Ar has been demonstrated to be a prolific β-delayed $2p$ emitter [2,3]. The mechanism of the β-delayed $2p$ decay in ^{31}Ar was studied in detail in two experiments at ISOLDE in 1995 [4] and 1997 [5] and found to be mainly sequential emission. A simultaneous component is predicted [6], but there is still no experimental evidence for it. With the setup used in the experiment presented here, which had a high efficiency for proton detection with a good energy and angular resolution, the decay of ^{31}Ar can now be used to study another exotic decay mode; β-delayed $3p$ emission, which has previously only been observed in two other nuclei, ^{45}Fe [7] and ^{43}Cr [8,9], while this decay mode only recently was discovered in the decay of ^{31}Ar by Pfützner *et al.* [10]. The study of ^{31}Ar can therefore now be used to bring the same level of information on this decay mode as it brought to the $\beta 2p$-decay mode roughly 15 y ago.

A detailed mapping of the $\beta 3p$-decay mode is needed to evaluate the β strength at high energy. Precise measurement of the $\beta 3p$ channels will also make it possible to reassign decays that have previously been wrongly assigned as $\beta 2p$ decays and thus the strength can be correctly placed in the decay scheme. Correct assignment of $2p$ events also requires a good detection efficiency for γ rays, which enables detection of $2p\gamma$ events and correct identification of the final state of the $2p$ decay in ^{29}P.

Owing to the sequential nature of the $2p$ decay it can be used to study levels in ^{30}S above the proton threshold, which are relevant for nuclear astrophysics. Experimental limits on the ratio between the proton and γ partial widths have been found for low-lying levels in ^{30}S using the $\beta 2p$ decay of ^{31}Ar from the same experiment discussed below [11]. As demonstrated here, the $2p$ decay mode can also be used to determine level spins by analyzing proton-proton angular correlations. Until now only tentative spin assignments have been suggested by

*Present address: Institut für Kernphysik, Technische Universität Darmstadt, D-64289 Darmstadt, Germany.
†Present address: Cyclotron Institute, Texas A&M University, College Station, TX 77843-3366, USA.

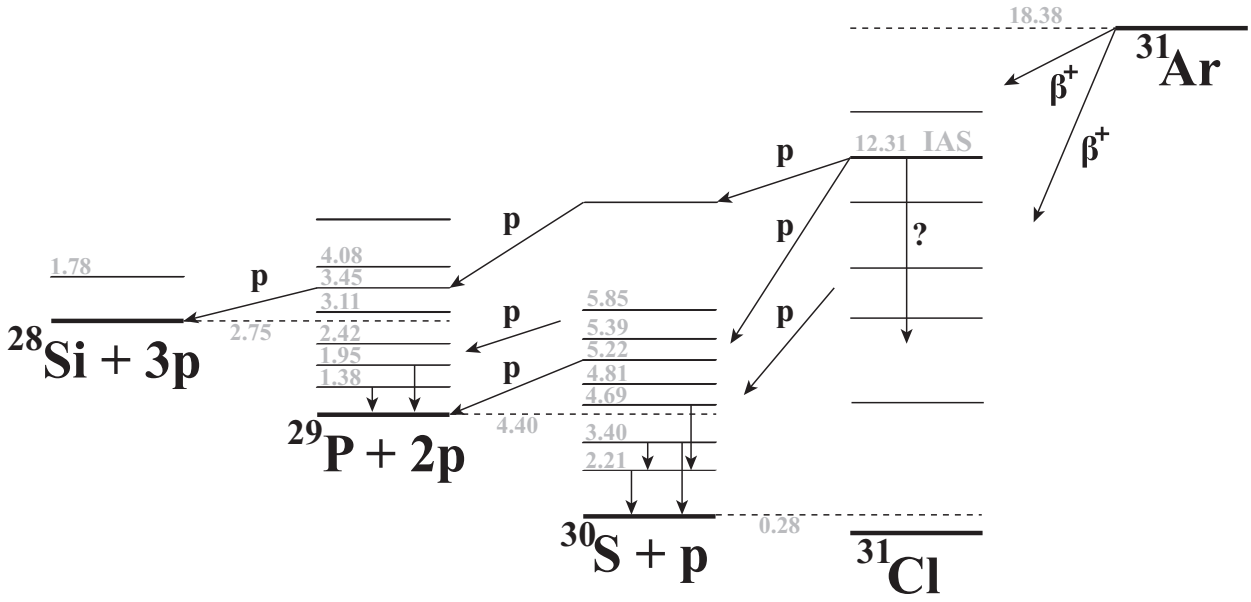

FIG. 1. Decay scheme for the β decay of ^{31}Ar, not to scale. Selected proton and γ transitions are drawn.

reference to assignments in the mirror nucleus [12]. A separate analysis of the Gamow-Teller strength using the $\beta 3p$ decay of ^{31}Ar is in preparation [13].

In Sec. II the experiment is described. Section III A describes the determination of the half-life of ^{31}Ar; an analysis of the spectroscopy of the $\beta 3p$-decay mode follows in Sec. III B. The analysis of the $\beta 2p\gamma$ events is presented in Sec. III C. The new, improved results on the Fermi strength is given in Sec. III D. The new method for finding the spin of low-lying levels in ^{30}S is presented in Sec. III E and applied to the case of the 5.2-MeV level, which lacks firm spin assignment. Finally in Sec. III F the γ transitions in the decay of ^{33}Ar are discussed, including identification of a previously unidentified γ line from the isobaric analog state (IAS). In Sec. IV the main results are summarized.

II. THE EXPERIMENT

The experiment was performed at the ISOLDE facility at CERN, Switzerland, using the ISOL technique [14] with a powder CaO target and a versatile arc discharge plasma ion source [15]. The 60-keV ion beam was guided through the General Purpose Separator [14] to separate the desired argon isotope from other produced nuclei. However, a significant background from nitrogen (as N_2 and N_2H) was present in the final beam. An average yield of ^{31}Ar of about 1 ion per second was obtained for a run time of 7 days. The beam was collected in a 50 $\mu g/cm^2$ carbon foil situated in the middle of the silicon cube detector setup [16]. The silicon cube consists of six double-sided silicon strip detectors (DSSSDs) in a cube formation; see Fig. 2. For this experiment one detector with thickness of 69 μm (No. 1), one detector with a thickness of 494-μm (No. 5), and four detectors with a thickness close to 300 μm (Nos. 2, 3, 4, 6) were used, with 1500-μm-thick 50×50-mm unsegmented silicon-pad detectors used for backing behind four of the detectors (Nos. 1, 2, 3, 6).

The geometry and energy calibrations of the DSSSDs were made using a beam of ^{33}Ar produced from the same target-ion source unit as ^{31}Ar. A comprehensive description of the setup can be found in Ref. [11]. The pad detectors behind the DSSSDs were energy calibrated by using a standard α calibration source (containing ^{148}Gd, ^{241}Am, ^{239}Pu, and ^{244}Cm). The total proton detection efficiency, ϵ_p, is taken as the total solid angle of the silicon Cube, which is 43(2)% of 4π.

Two Miniball germanium cluster detectors [17] were situated outside the cube chamber behind detectors 3 and 4. Each Miniball cluster consists of three crystals, but unfortunately one of the crystals of the cluster behind

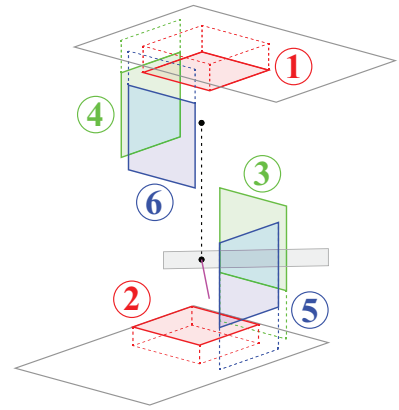

FIG. 2. (Color online) The detector setup used for the experiment consisting of a cube of DSSSDs and two Miniball Ge detectors. The beam enters between DSSSDs 5 and 6 and is stopped in a carbon foil mounted on a small metal holder entering between DSSSDs 3 and 5. The top of the cube with three of the DSSSDs is lifted, following the dotted black line, for better visualization. The two Miniball detectors that were situated outside the cube behind DSSSDs 3 and 4 are not shown in the picture.

DSSSD 3 gave no signal. A preliminary energy calibration was made using ^{137}Cs and ^{60}Co. This was supplemented by a ^{152}Eu source together with high energy γ lines from the decay of ^{16,18}N, ^{15}C, and ^{32,33}Ar recorded on-line. Together, this gives an energy calibration up to an energy of 2.5 MeV with an uncertainty of 1 keV, while above this energy, the uncertainty is estimated to be 3 keV.

A total efficiency calibration was made for the two Miniball detectors. First, an absolute efficiency calibration was made using the low-lying γ lines from a ^{133}Ba source with a known activity of 17.0(3) kBq at the time of the experiment. The detection efficiency for the γ lines from the ^{152}Eu source, corrected for emission probabilities using [18], is then scaled, using the 302- and 356-keV points from ^{133}Ba and placing the 344-keV point from ^{152}Eu on a straight line between these. The absolute γ efficiency above 600 keV was then found by fitting the ^{152}Eu points to a relative efficiency curve determined in a slightly different detector configuration [19] (that used four different γ sources: ^{152}Eu, ^{60}Co, ^{207}Bi, and ^{11}Be). The result, using the formula in Ref. [20], is

$$\varepsilon_\gamma(E) = 0.21 \exp\left\{-2.669 - 1.457 \log_{10}\left(\frac{E}{\mathrm{MeV}}\right) - 0.231\left[\log_{10}\left(\frac{E}{\mathrm{MeV}}\right)\right]^2\right\}, \quad (1)$$

with an estimated uncertainty of 10%.

For normalization of the total number of ^{31}Ar collected during the run, the largest one-proton peak at 2083 keV with an absolute branching ratio of 26.2(29)% [21] is used. A small fraction of the activity could only be seen from the beam entrance side. Furthermore, the target holder shadows several pixels in particular for detectors 1 and 2. These effects are all included in the detailed Monte Carlo simulations discussed below to extract final branching ratios. It is estimated that the total number of ^{31}Ar collected during the experiment is $5.6(6)\times10^5$.

III. RESULTS AND DISCUSSION

A. Half-life of ^{31}Ar

The half-life of ^{31}Ar is found in the same way as in Ref. [5]. Data were recorded continuously, but only events happening after the beam gate was closed 100 ms after each proton impact on the production target were considered for the half-life determination. Only the strongest $1p$ peak at 2083 keV, corresponding to an energy range between 2040 and 2120 keV, was used to minimize background contributions. In this way the data could be fitted using the maximum likelihood method to a single exponential component and a constant background. This gave a half-life of 15.1(3) ms, which is consistent with previous determinations of 14.1(7) [5], 15(3) [3], and $15.1^{+1.3}_{-1.1}$ ms [22].

B. β-delayed three-proton spectroscopy

In the following we present the first spectroscopic analysis of a β-delayed three-proton decay. A spectrum of the Q_{3p} values calculated for the $3p$ events observed during the experiment is shown in Fig. 3. To eliminate contamination

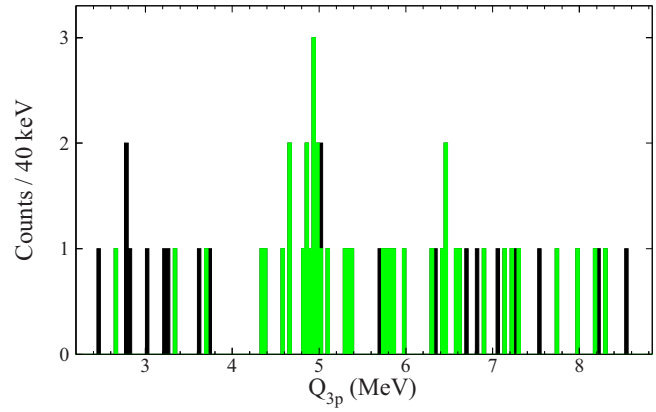

FIG. 3. (Color online) Q_{3p} for three-particle events. The histogram shows all the events where the first two particles detected have energies above 800 keV and the third has an energy above 500 keV unless it is in detector 5, where it also has to have an energy above 800 keV. To obtain the histogram in green (gray), events that are most likely not real $3p$ events were removed as described in the text.

from noise and β particles the following energy gates are used: The energy of the first two particles detected should exceed 800 keV and the energy of the third 500 keV unless it is in the thick detector (detector 5), where a β particle can deposit more energy. In the latter case the gate is set at 800 keV. The reason for allowing the third particle to have an energy less than the others is that the $3p$ decay could go through the 3447.6(4)-keV $\frac{7}{2}^-$ level in ^{29}P 699 keV above the proton threshold. In principle, the decay can also go trough the 3105.9(3)-keV $\frac{5}{2}^+$ level only 357 keV above the proton threshold. However, the penetrability for this level is roughly a factor of 25 below the penetrability for the $\frac{7}{2}^-$ level. Furthermore, it is not possible with our setup to distinguish these low-energy protons from β particles. We thus first assume that there are no transitions through the $\frac{5}{2}^+$ level. At the end of this section we return to this issue and argue that this is a good assumption.

The efficiency of detecting a β particle in coincidence with a proton, using the same analysis cuts as for protons, can be estimated to be 0.43(5)% from events with a single proton and a β particle. Using this efficiency we deduce from the measured number of $2p$ event an expected number of $\beta 2p$ events of 29(4), roughly half of the total number of three-particle events of 62. Some of these background events can be identified if the Q_{2p} value of two of the particles corresponds to one of the prominent two-proton transitions as was earlier demonstrated in Ref. [23]. Also, some of the three-particle events are all in the same detector or have a too high Q_{3p} value. In this way 21 background events can be identified and removed, and only the 41 remaining events are included in the following analysis. These events are shown as the green (gray) histogram in Fig. 3.

A peak is seen in the green (gray) histogram of Fig. 3 around 4.89(29) MeV containing 19 events (between 4.3 and 5.5 MeV). To investigate the spread in Q_{3p} owing to detection resolution a simulation was made, which showed that the expected full width at half maximum is more than 300 keV. A real peak of events from a given level in ^{31}Cl is thus expected

to be as broad as the one at 4.89(29) MeV. This peak is most likely attributable to the $3p$ decay of the IAS, because it corresponds to a ^{31}Cl level at an energy of 12.32(29) MeV. It is interesting to note that it is only approximately half of the $3p$ events that belong to the decay of the IAS. The other half stems from transitions from levels in ^{31}Cl above the IAS. Owing to the large Q window for particle emission, many decay channels are open; only a small fraction will therefore decay by two-proton emission to the ground state in ^{29}P. To make a correct assignment, detection of $3p$ and $2p\gamma$ branches is required. Using now the $\beta 3p$ decay a better determination of the Gamow-Teller strength at high energy can be performed. The $3p$ spectrum is discussed in detail separately in Ref. [13].

The mechanism of the β-delayed $3p$ emission from the previously studied nuclides has not been determined. If sequential emission occurs in the case of ^{31}Ar, it should be possible to identify the known levels in both ^{30}S and ^{29}P from the energy of the protons. However, owing to limited statistics and the considerable level density for high excitation energies in ^{30}S, it will not be possible to do this for ^{30}S. If the decay goes through levels in ^{29}P, these can be identified via the difference between the Q_{3p} value and the Q_{2p} value, because this difference corresponds to the energy of the level populated in ^{29}P minus the proton separation energy. The reason for using the two Q values is that these can be extracted directly from the experimental data and that a correction for the recoil of the daughter nucleus is included. The Q_{3p} value can be calculated independently of the decay mechanism, while for the Q_{2p} value one must choose which particles should be considered to be the first two in the decay. In Fig. 4 this difference is plotted for two different choices together with lines indicating the levels in ^{29}P. For the black dots it is assumed that the first two particles are the ones with the highest energy. This is, however, not necessarily a reasonable assumption for all the events. Instead, the first two particles can be chosen so that the difference between the Q_{3p} and the Q_{2p} values fits the known levels in ^{29}P (only the first five levels were included). This choice is plotted as the green (gray) triangles. This analysis

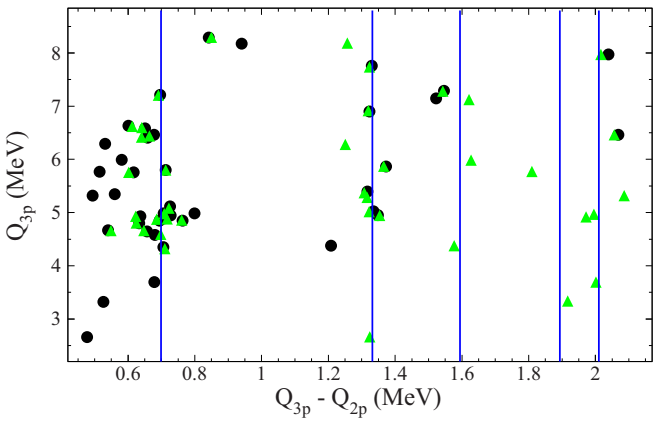

FIG. 4. (Color online) Q_{3p} vs $Q_{3p} - Q_{2p}$. The lines indicate the levels in ^{29}P. For the black circles Q_{2p} is calculated assuming that the first two particles are the ones with the highest energy and for the green (gray) triangles it is calculated to best fit the five levels in ^{29}P shown.

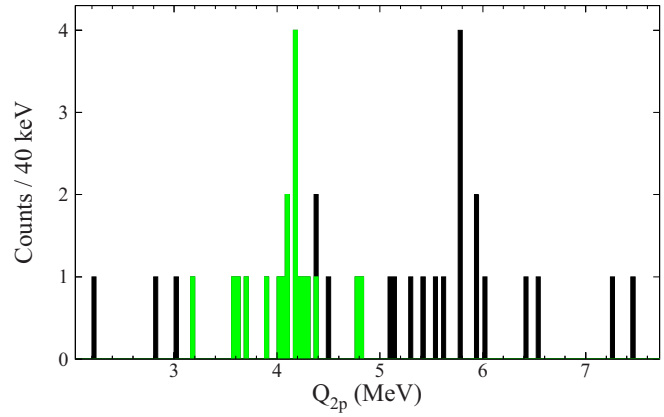

FIG. 5. (Color online) Q_{2p} calculated from the two particles with highest energy. The histogram is from the 41 events in the green (gray) histogram of Fig. 3. The part that is green (gray) is the 19 events around 4.84(29) MeV in the green (gray) histogram of Fig. 3.

suggests that the $3p$ emission is consistent with being fully sequential, but owing to the large expected spread in the Q_{3p} value a considerable simultaneous emission contribution cannot be excluded. When the energies of all three particles are above 1.2 MeV, the particles are most likely all protons, but the density of states in ^{29}P is then so high that it is easy to interpret a simultaneous decay as a sequential decay. This is not a problem for the level at 3447.6(4) keV (corresponding to a difference between Q_{3p} and Q_{2p} of 699 keV). The problem here is that one of the particles has an energy around 0.7 MeV and it is thus difficult to distinguish protons from β particles. The majority of these events stem from the peak in the Q_{3p} spectrum around 4.89(29) MeV (see Fig. 3), which most likely belongs to the decay of the IAS. Their Q_{2p} value can be seen in Fig. 5: More than half of them lie around 4.14(13) MeV. Assuming they go through the 3447.6(4)-keV level in ^{29}P, this corresponds to a ^{31}Cl energy at 12.27(13) MeV, in complete agreement with the value of 12.32(29) MeV from the Q_{3p} value. These events cannot be $2p\beta$ events; if they were, one would expect more than 2×10^3 events at this energy in the Q_{2p} spectrum made from $2p$ events. While there are indications of small peaks around this energy, they contain less than 70 events. The IAS $3p$ decay can thus be assigned partly to go through the level at 3447.6(4) keV in ^{29}P, which supports the assumption that the events lying close to 699 keV in Fig. 4 also are events going through this level.

We have also strong indications of events going through the level at 4080.5(3) keV (corresponding to a difference between Q_{3p} and Q_{2p} of 1332 keV). With the statistics available here and the expected large spread in the Q_{3p}, this is, however, not conclusive. The sparsity of events with $Q_{3p} - Q_{2p}$ between 0.9 and 1.1 MeV is a strong indication that there are no simultaneous $3p$ decays with a low-energy proton.

We now return to the issue of possible involvement of the $\frac{5}{2}^+$ level at the 3105.9(3)-keV level 357 keV above the proton threshold. By using measurements of the resonance strength, $(2J+1)\frac{\Gamma_p\Gamma_\gamma}{\Gamma}$, and the lifetime [24] one finds for the $\frac{7}{2}^-$ level that $\Gamma \sim \Gamma_{\max} = 51(31)$ meV and $\Gamma_{\min} = 0.038(10)$ meV, where $\Gamma_{\max}$ ($\Gamma_{\min}$) refers to the largest (smallest) width of Γ_p

and Γ_γ. For the $\frac{5}{2}^+$ level one finds $\Gamma \sim \Gamma_{\rm max} = 19(9)$ meV and $\Gamma_{\rm min} = 0.46(11)$ meV. If $\Gamma_{\rm max} = \Gamma_\gamma$ for the $\frac{7}{2}^-$ level, one would expect to see around 700 γ rays at 1493.6 keV, corresponding to the decay of this level to the second excited level, when gating on two protons. This we do not see in our two-proton-gated γ spectrum; see Sec. III C and Fig. 7. We therefore conclude that $\Gamma_p = \Gamma_{\rm max}$. Looking now at the mirror nucleus ^{29}Si, where the $\frac{7}{2}^-$ and $\frac{5}{2}^+$ levels both lie below the proton threshold, we see that the half-lives of these two levels are 2.63(9) ps and 33(1) fs, respectively. The half-lives of the two levels in ^{29}P are 9(6) fs and 23(10) fs, respectively. By comparison it is reasonable to assume that $\Gamma_p = \Gamma_{\rm max}$ for the $\frac{7}{2}^-$ level, as deduced above, and $\Gamma_p = \Gamma_{\rm min}$ for the $\frac{5}{2}^+$ level. From this it is found that the proton width of the $\frac{5}{2}^+$ level is 111(72) times smaller than the proton width of the $\frac{7}{2}^-$ level and it is thus reasonable to assume that the $3p$ decay through the $\frac{5}{2}^+$ level is suppressed.

C. β-delayed $2p\gamma$-decay

The indications of a sequential $3p$ branch implies that the decay populates higher-lying levels in ^{29}P than previously found. With our setup it was possible to detect γ rays in coincidence with protons and we thus have a chance to see the γ transitions from these levels. However, the detection efficiency is limited and the chance of detecting the γ ray in coincidence with both of the emitted protons is thus very small. For a real $2p\gamma$ event it is $2/\epsilon_p = 4.6$ times more likely to detect it as a $1p\gamma$ event than to detect it as a $2p\gamma$ event. We therefore first search for the transitions from higher-lying levels in ^{29}P in the one-proton-gated γ spectrum, which is shown in Fig. 6. (As previously, 800 keV is used as a lower energy cut on the proton). In this spectrum clear peaks are identified from the lowest states of both ^{30}S and ^{29}P (see Ref. [11]), but owing to background in the spectrum there are no clear signatures of levels above the second excited state in ^{29}P. In Fig. 7 the two-proton-gated γ spectrum is shown. Two different gates are used: one where both particles have energies above 800 keV (black) and one where the second particle has an energy above 500 keV unless it is in the thick detector 5, where it is required

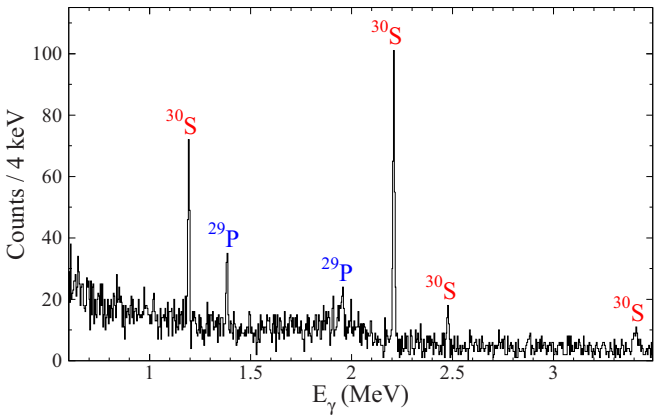

FIG. 6. (Color online) The γ spectrum gated on one proton with an energy above 800 keV.

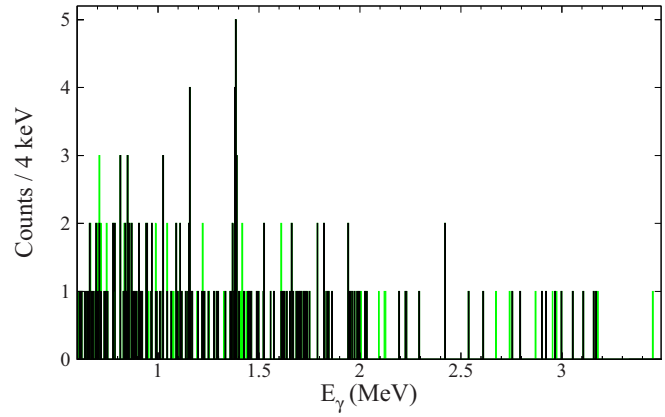

FIG. 7. (Color online) The γ spectrum gated on two protons. For the black spectrum both protons have energies above 800 keV. The extra events in green (gray) are γ rays where one of the protons has an energy between 500 and 800 keV and has not hit detector 5.

to be above 800 keV [black + green (gray)]. In the following all the levels in ^{29}P up to 4.1 MeV are considered and the number of $2p\gamma$ events is compared with the one expected from the $1p$-gated γ spectrum. Because there is no reason why the second emitted proton should have an energy above 800 keV instead of just 500 keV, the extra events in green (gray) in Fig. 7 are also included.

We now discuss in turn the evidence for the γ rays from the relevant states in ^{29}P. The first excited state in ^{29}P($\frac{3}{2}^+$) is at 1383.55(7) keV [24]. The corresponding peak is clearly seen in both the $1p$- and $2p$-gated γ spectra. There are 64(11) events above background in the $1p$-gated spectrum. This implies that there should be 14(2) events in the $2p$-gated spectrum, which agrees very well with the 13(4) measured above background.

The second excited state at 1953.91(17) keV ($\frac{5}{2}^+$) decays primarily to the ground state. A peak at this energy is seen in the $1p$-gated γ spectrum. It contains 59(15) events, but it is more than twice as broad as the other peaks in the spectrum. This and the discussion in Ref. [11] indicates that there might be other contributions to the peak. From the 59(15) events in the $1p$-gated spectrum one would expect 13(3) events in the $2p$-gated spectrum. Only 7(3) events are observed in total, but if there are other contributions to the peak in the one-proton-gated spectrum the expected number would be smaller.

The third excited state is a $\frac{3}{2}^+$ state at 2422.7(3) keV, and it decays also primarily to the ground state. There is no significant signal above background in the $1p$-gated γ spectrum at this energy. In the $2p$-gated spectrum there are two events with no significant background at 2422(11) keV. This would imply 9(7) events in the $1p$-gated spectrum. Considering the background level in this area in the $1p$-gated spectrum it is not possible to disprove this.

The next level is the 3105.9(3)-keV level, which is just above the proton threshold. It is a $\frac{5}{2}^+$ level and decays primarily by a 1722.2-keV γ ray. Again there is no significant signal above background in the $1p$-gated spectrum. There are a maximum of 14(9) events above background, which implies there should be 3(2) events in the $2p$-gated spectrum, where there are a total of 2.

The $\frac{7}{2}^-$ level at 3447.6(4) keV, which was identified in the $3p$ decay, has a total half-life of 9(6) fs. It decays primarily by a 1493.6-keV γ ray. There is a hint of a peak in the $1p$-gated γ spectrum at this energy containing 14(7) events. From this one expects 3.0(15) events in the $2p$-gated spectrum, where there are a total of 2.

The level at 4080.5(3) keV is a $\frac{7}{2}^+$ level with a total half-life of 11(1) fs. It decays primarily by a 2126.3-keV γ-ray. In the $1p$-gated γ spectrum, there is no indication of a peak at this energy. There are 5(5) events, which means that there should be 1(1) event in the $2p$-gated spectrum and there are a total of 2 events.

In summary, the γ decays observed for the six lowest levels in ^{29}P give consistent results for the $1p$- and $2p$-gated γ spectra, but only the feeding of the lowest two can be seen directly in the γ spectra.

D. The Fermi strength of the β decay

The Fermi strength in the β decay of ^{31}Ar has been measured previously [5] by considering the $1p$ and $2p$ decays of the IAS to the lowest states in ^{30}S and ^{29}P. As shown in Ref. [11] and in the results presented above for the IAS, there are additional contributions. In addition to the $3p$ channel, all the levels up to the vicinity of the proton thresholds should, in principle, be included for both the $1p$ and the $2p$ channels. To get a precise determination of the branching ratios for the different channels it is important to use spectra with a good energy resolution and to precisely know the total number of ^{31}Ar collected and the detection efficiencies. For this reason only the 300-μm DSSSDs with backing are selected for this analysis. Of these, detector 2 had several broken strips and less accurate efficiency determination owing to shading from the target holder. This leaves only detectors 3 and 6, which are used to determine the branching ratios for the two- and one-proton decays in the following. The statistics is so low for the three-proton decay that all the detectors are needed, and the branching ratio is thus found using the data presented in Sec. III B. It is listed in Table I together with the branching ratios found for the two- and one-proton decays. The branching ratio found here for the three-proton decay to the ground state of ^{28}Si is consistent with the 99% confidence level upper limit of 0.11% found by Fynbo *et al.* [23].

TABLE I. Branching ratios for the decay of the IAS. The ^{31}Cl energies are found using the masses from Ref. [27] and a proton separation energy for ^{31}Cl of 282.8(44) keV [28]. The decays written in *italic* correspond to decays not uniquely identified in the spectra: There is marginal indication of the two-proton branch and the one-proton branches cannot be uniquely assigned to levels in ^{30}S. The total branching ratio is quoted with and without these decays. The efficiencies used are different for each of the three decay modes and the uncertainties stemming from these are included in the uncertainties for each decay. The correlation is taken into account for the uncertainty on the total branching ratio. Furthermore, there is a systematic error of 11% stemming from the normalization (see Sec. II), which is not included in the uncertainties.

Three-proton branch				
Final state in ^{28}Si(keV)	J^π	Q_{3p}(MeV)	E_{IAS}(MeV)	B.R. (%)
0	0^+	4.89(29)	12.32(29)	0.039(19)
Two-proton branch				
Final state in ^{29}P(keV)	J^π	Q_{2p}(MeV)	E_{IAS}(MeV)	B.R. (%)
0	$\frac{1}{2}^+$	7.633(4)	12.311(6)	1.47(23)
1383.55(7)	$\frac{3}{2}^+$	6.251(4)	12.313(6)	0.88(15)
1953.91(17)	$\frac{5}{2}^+$	5.688(6)	12.320(8)	0.40(10)
2422.7(3)	$\frac{3}{2}^+$	*5.22(8)*	*12.32(8)*	*0.075(50)*
One-proton branch				
Final state in ^{30}S(keV)	J^π	E_p(MeV)	E_{IAS}(MeV)	B.R. (%)
0	0^+	11.57(8)	12.24(8)	0.049(11)
2210.2(1)	2^+	9.46(8)	12.27(8)	0.104(18)
3404.1(1)	2^+	8.33(8)	12.30(8)	0.108(17)
3667.7(3)	0^+	*8.08(8)*	*12.30(8)*	*0.101(21)*
3677.0(3)	1^+		*12.31(8)*	
4687.7(2)	3^+	*7.01(8)*	*12.22(8)*	*0.38(4)*
4809.0(3)	2^+		*12.34(8)*	
Total			12.313(4)	3.05(42)
Total				*3.60(44)*

The two-proton spectrum using only detectors 3 and 6 (with $E > 500$ keV) is shown in Fig. 8. The peaks corresponding to the decay to the ground state and the first and second excited states of ^{29}P are clearly visible in the spectrum at Q_{2p} values of 7.6, 6.3, and 5.7 MeV. There is possibly a peak at 5.2 MeV corresponding to the transition to the third excited state in ^{29}P. Transitions to higher-lying states cannot be identified. The branching ratios in Table I are all lower than those reported by Fynbo *et al.* [5]. The main reason for this is that our energy and angular resolution is better for this energy range, making our peaks significantly narrower. Reference [5] therefore included contributions from decays with Q_{2p} values close to those for the IAS decays. Furthermore, for the decays to excited states in ^{29}P, the background from Gamow-Teller transitions is estimated and subtracted here, which was not done in Ref. [5].

The one-proton energy spectrum for detector 3 can be seen in Fig. 9 (the spectrum for detector 6 is similar). The branching ratios are found separately for detectors 3 and 6 and the average is given in Table I. The large uncertainty

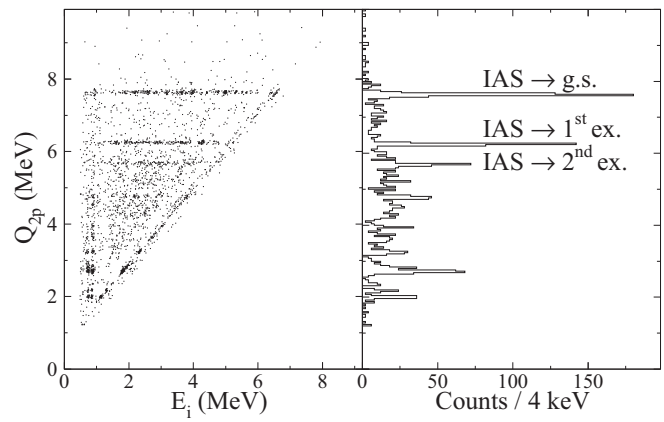

FIG. 8. Two-proton spectrum made using only detectors 3 and 6 with a lower cutoff of $E > 500$ keV. (Left) Q_{2p} vs the energy, E_i, of the two particles. (Right) The projection onto the Q_{2p} axis.

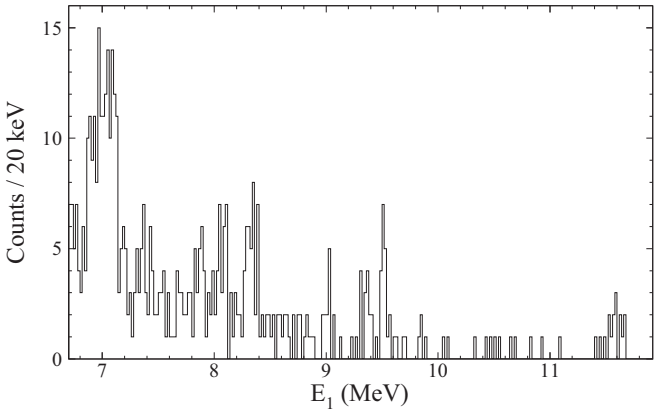

FIG. 9. The one-proton energy spectrum for detector 3 for high energies.

in the energy is attributable to limited statistics and a large uncertainty in the calibration of the back detectors for high proton energies. Because the energy cutoff of the two-proton spectra is 500 keV the branching ratios are given up to the ^{30}S level at 4809.0(3) keV [11] (413 keV above the proton threshold) in the one-proton spectrum. The peaks at 8.1 and 7.0 MeV cannot be separated into two components, even though they should both contain contributions from decays to two different levels in ^{30}S. The branching ratios are thus found for the total contribution from the two levels.

If we neglect isospin symmetry breaking the β strength to the IAS is $B_F = 5$. Using the Coulomb displacement energy of ^{32,33,34,35}Ar extracted from Ref. [25] we estimate the Coulomb displacement energy of ^{31}Ar to be 6.85(10) MeV, giving $Q_{\mathrm{EC}} = 18.38(10)$ MeV. With this and our improved half-life of ^{31}Ar (see Sec. III A) we obtain a total theoretical branching ratio of 4.24(43)%, where the large uncertainty stems from the uncertainty on the Q_{EC} value. Without this the uncertainty of the total theoretical branching ratio is only 0.09%. A better determination of the mass of ^{31}Ar would thus be very beneficial. The theoretical branching ratio is larger than the experimental value of 3.60(44)%, but the discrepancy is within one standard deviation. The uncertainty on the experimental value cited does not include the relatively large uncertainty stemming from the normalization of the number of ^{31}Ar ions in the experiment determined by using the absolute branching ratio of the main $1p$ peak (see Sec. II). The results here constitute an improvement over the earlier result by Fynbo *et al.* [5], but note that the uncertainties on both the total experimental and theoretical branching ratios quoted there are underestimated. However, there remain levels in ^{29}P below the proton threshold and one above to which two-proton decays could not be extracted. We could also not identify any γ rays corresponding to transitions in ^{31}Cl from the IAS, but a contribution from these cannot be excluded. Note that γ transitions from the IAS have been found in the decay of both ^{32}Ar [26] and ^{33}Ar (see Sec. III F).

E. Spin of low-lying levels of ^{30}S

A detailed knowledge of the levels just above the proton threshold in ^{30}S is important for determining the reaction rate of ^{29}P$(p,\gamma)^{30}$S, which influences the silicon abundances that can be directly studied from presolar dust grains believed to be produced in classical novae. In the last few years the relevant levels in ^{30}S have been studied intensely [11,12,29–31], such that the energies are now known for the relevant levels, while some disagreements about the spin assignment remain. In this section we present a new method for determining the spin of these levels. The method is used to give the first determination of the spin of the 5.2-MeV level populated in the ^{31}Ar decay.

The method is based on using the sensitivity on spin of proton-proton angular correlations in $2p$ decays going through the level of interest. The distribution of angles, θ, between the two protons can be written as [32]

$$W(\cos\theta) = \sum_{\nu=0}^{\nu_{\max}} A_\nu P_\nu(\cos\theta),$$

where P_ν is the νth Legendre Polynomial and the sum extends to

$$\nu_{\max} = \min(2l_1, 2l_2, 2j),$$

so that one obtains an isotropic distribution if the angular momenta involved are small enough. Here $j_1(l_1)$ and $j_2(l_1)$ are the spin (orbital angular momentum) of the first and second emitted protons, respectively, and j is the spin of the ^{30}S state coupled with the first proton. The coefficient A_ν is given by

$$A_\nu = F_\nu(l_1, j_1, j)\, b_\nu(l_1, l_1)\, F_\nu(l_2, j_2, j)\, b_\nu(l_2, l_2)$$

$$b_\nu(l, l') = \frac{2\sqrt{l(l+1)l'(l'+1)}}{l(l+1) + l'(l'+1) - \nu(\nu+1)},$$

where F_ν can be found from the tabulation in Ref. [32].

In the $\beta 2p$ decay of ^{31}Ar we expect the excess protons to be mainly in the sd shell and shall therefore make the assumption that only positive parity states in ^{30}S will be populated. The possible values for A_2 in the decay are given in Table II. In many cases there are two possible values for j and the table indicates the range spanned by the two extreme situations in which only one j value contributes.

To use this method, transitions from distinct levels in ^{31}Cl must be identified with sufficient statistics. This is only possible for the strongest fed level in ^{30}S at 5.2 MeV. This level has previously been assigned either as 0^+ [12] based on levels in the mirror nucleus or as a 3^+ state based on its γ decay [29]. To have sufficient statistics all detectors are used with a low-energy cutoff on the first particle of 800 keV and the second of 500 keV, except for the thick detector 5, where

TABLE II. The A_2 coefficients for $2p$ transitions calculated for the different initial states, J_i^π (in ^{31}Cl), through five positive parity states, J_m^π (in ^{30}S), to a $\frac{1}{2}^+$ final state (ground state of ^{29}P).

$J_m^\pi\, J_i^\pi$	$\frac{3}{2}^+$	$\frac{5}{2}^+$	$\frac{7}{2}^+$
0^+	0	0	0
1^+	0	0	0
2^+	0	0	[−0.70; −0.25]
3^+	[0.15; 0.87]	0	0
4^+	[0.76; 1.00]	[0.13; 0.95]	0

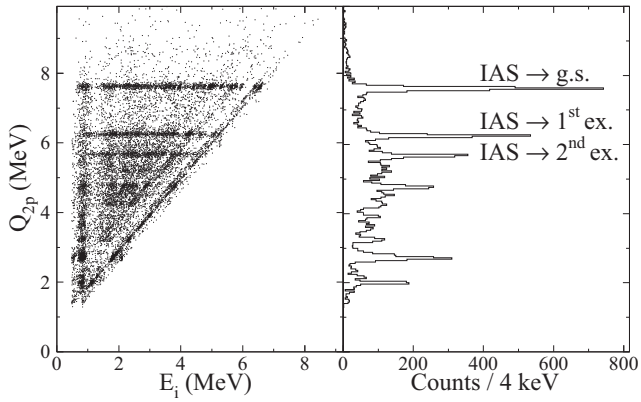

FIG. 10. Two-proton spectrum with lower cutoff, $E_1 > 800$ keV and $E_2 > 500$ keV, except for detector 5, where $E_2 > 800$ keV. (Left) Q_{2p} vs the energy, E_i, of the two particles. (Right) The projection onto the Q_{2p} axis.

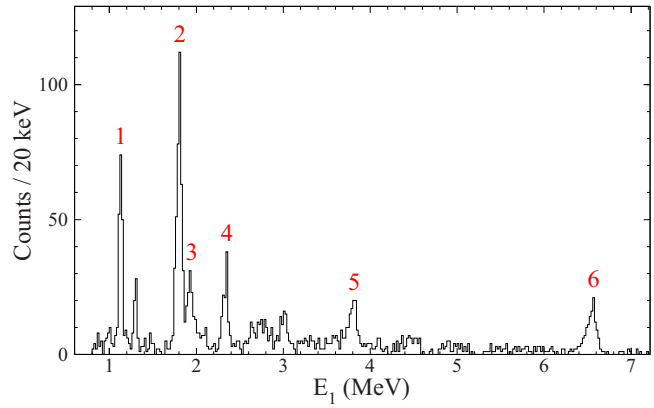

FIG. 12. (Color online) Energy of the first particle for transitions going through the 5.2-MeV level in ^{30}S. The peaks containing most counts are marked by numbers.

800 keV is used. The resulting data are shown in Fig. 10. The ^{30}S levels calculated from these events can be seen in Fig. 11. The energy of the first particle (the one with the highest energy) of the events passing through the 5.2-MeV level are shown in Fig. 12. Each peak in this spectrum corresponds to population of the 5.2-MeV level from specific states in ^{31}Cl. The most intense peaks are numbered and are used in the following analysis. In Fig. 13 the angular correlation for two of the peaks are shown together with a simulation of the same decay that assumes a uniform angular distribution (i.e., $A_2 = 0$). The simulated curves are fitted to the data for all numbered peaks of Fig. 12 with and without an A_2 term. The resulting A_2 values are shown in Table III along with the difference in χ^2 for the two fits. Also shown are the results of a Kolmogorov test (essentially the maximum difference in cumulative distributions scaled with the square root of the number of counts; the 5% significance level then corresponds to a value of 1.36 [33]) for a comparison between the data and a uniform distribution.

Both the χ^2 difference and the Kolmogorov test indicate that the events in peaks 1, 5, and 6 are consistent with being uniform. The conclusion for peaks 2 and 3 is less clear: The Kolmogorov test shows with 97.5% confidence that the events in peak 2 are not consistent with a uniform distribution [33], but the deviations do not correspond to a standard angular correlation shape because the fit does not give a value for A_2 that is significantly different from 0 (fits including an

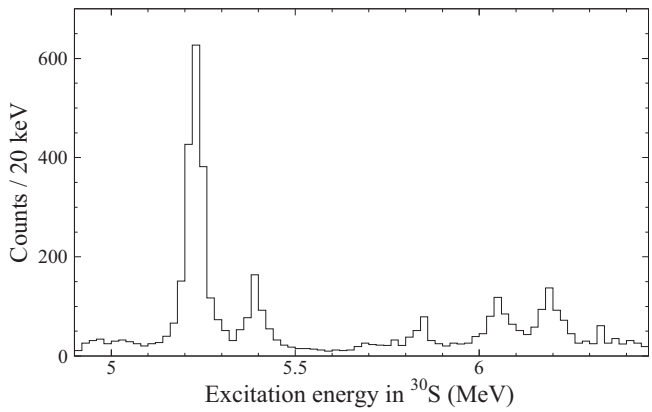

FIG. 11. Energy spectrum for ^{30}S calculated for the events from Fig. 10.

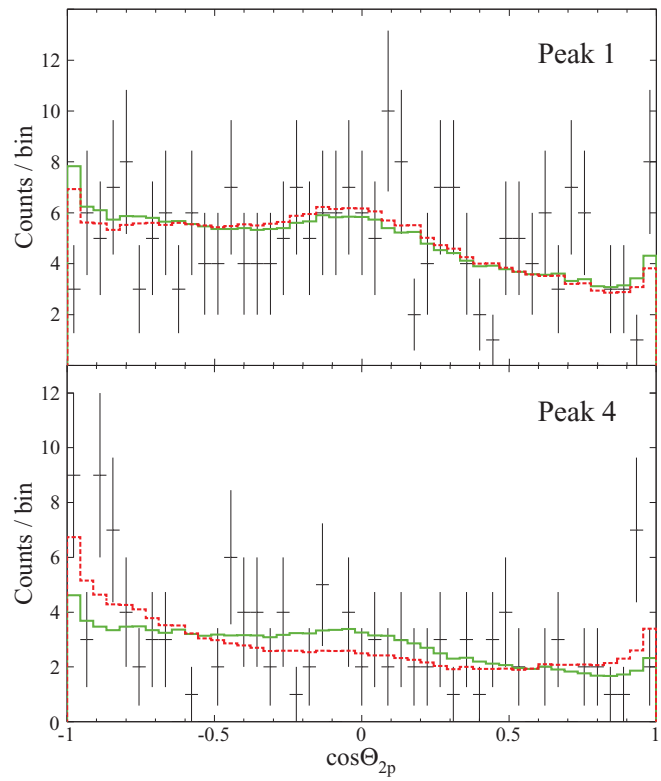

FIG. 13. (Color online) Angular distribution of the two protons forming peaks 1 and 4 in Fig. 12 compared with the corresponding fitted $2p$ simulations for either isotropic (green solid curve) or nonisotropic (red dashed curve) distributions. For better visualization data are here shown using 45 bins, while the fits are made using 90 bins.

TABLE III. The A_2 coefficients for different $2p$ transitions from ^{31}Cl through the 5.2 MeV level in ^{30}S, together with the difference in χ^2 compared to a uniform fit and the result D of a Kolmogorov test to a uniform distribution. The peak numbers correspond to Fig. 12.

Peak	$E(^{31}\mathrm{Cl})$ (MeV)	A_2	$\Delta\chi^2$	D
1	6.674(6)	−0.12(14)	0.67	0.79
2	7.380(6)	0.16(11)	1.97	1.57
3	7.512(7)	0.35(19)	3.51	0.88
4	7.919(8)	0.48(19)	6.69	1.40
5	9.434(9)	0.04(19)	0.05	0.72
6 (IAS)	12.313(4)	0.03(18)	0.03	0.65
All		0.18(5)	13.18	7.95

A_4 term do not change this conclusion). The fit for the events of peak 3 points to an A_2 parameter different from 0, but the Kolmogorov test does not find the distribution to be significantly different from uniform. Finally, the events of peak 4 have a distribution significantly different from uniform with more than 95% confidence [33] using the Kolmogorov test and the value for A_2 is different from 0 with more than 2σ. This is also the case if all events of the 5.2-MeV peak are considered, which implies that there must be components that are nonuniform. With reference to Table II this excludes the 0^+ and 1^+ assignments for the ^{30}S level. Spin 2^+ is also excluded because it can only give deviations to negative A_2 values.

The spins of the states in ^{31}Cl corresponding to the numbered peaks in Fig. 12 are only known for the case of the IAS (peak 6), where it is $\frac{5}{2}^+$. The other observed states can be either $\frac{3}{2}^+$, $\frac{5}{2}^+$, or $\frac{7}{2}^+$ assuming that only allowed β decays are populated. The A_2 value for the IAS indicates a uniform distribution. By comparing the value of A_2 with the A_2 values in Table II it can be concluded that the 5.2-MeV level in ^{30}S has spin 0–3^+, while the 4^+ assignment is less likely. By comparing the value of A_2 for peak 4 with Table II we can only conclude that this peak stems from a $\frac{3}{2}^+$ or $\frac{5}{2}^+$ level in ^{31}Cl. If

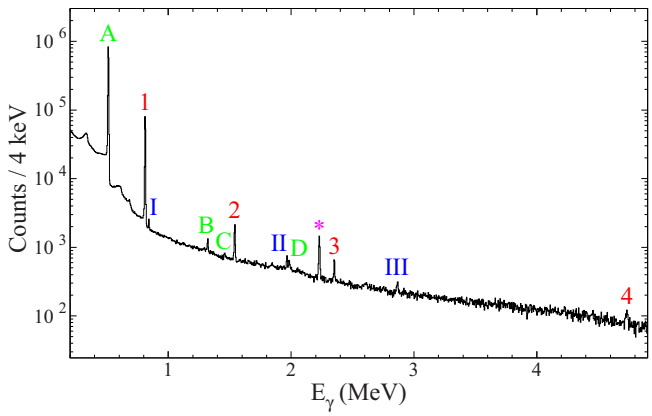

FIG. 14. (Color online) The γ spectrum of ^{33}Ar. The numbers corresponds to transitions in the β-daughter ^{33}Cl, the Roman numbers to transitions in the β-granddaughter ^{33}S and the * to a transition in the β-proton daughter ^{32}S. The letters corresponds to background lines.

TABLE IV. The relative branching ratios of the γ transitions in the decay of ^{33}Ar (above the line) and ^{33}Cl (below the line). The peak identifier corresponds to Fig. 14. The intensities of the γ transitions from the ^{33}Ar decay are normalized to peak 1 and compared to the results of Ref. [34]. The transition marked by a * is compared to Ref. [35], as suggested in Ref. [34]. The intensities of the γ transitions from the decay of ^{33}Cl are normalized to peak III and compared to the results of Ref. [36].

Peak	E_γ(keV)	I_γ	E_γ^{ref}(keV)	I_γ^{ref}
1	811.2(10)	100(10)	810.6(2)	100(1)
2	1541.0(10)	3.2(3)	1541.4(6)	3.6(2)
3	2342.3(11)	1.10(13)	2352.5(6)	1.3(2)
4	4734(3)	0.46(9)		
*	2230.4(19)	3.9(4)	2230.6(9)	1.7(5)
I	841.3(10)	109(16)	841	118.6(36)
II	1966.9(12)	132(18)	1966	104.2(16)
III	2867(3)	100(15)	2866	100.0(18)

peak 4 corresponds to a $\frac{5}{2}^+$ level the spin of the ^{30}S level must be 4^+, and if it is a $\frac{3}{2}^+$ level it most likely must be 3^+ while 4^+ is less likely. Considering in a similar way all the data in Table III, the preferred value for the spin of the 5.2-MeV level is 3^+, because several of peaks 1–6 give a uniform distribution, which for a 3^+ level would be consistent with both $\frac{5}{2}^+$ and $\frac{7}{2}^+$ levels in ^{31}Cl. One would expect at least one of peaks 1–6 to come from a $\frac{3}{2}^+$ level in ^{31}Cl and therefore a 4^+ assignment of the 5.2-MeV level would produce an angular correlation significantly different from uniform. Assuming that the spin of the 5.2-MeV level is 3^+, one can infer that the spin of the 7.919(8)-MeV level in ^{31}Cl (peak 4) is $\frac{3}{2}^+$ and that of the 6.674(6)-MeV level (peak 1) is either $\frac{5}{2}^+$ or $\frac{7}{2}^+$. The spin of the remaining three levels (excluding the IAS) cannot be restricted owing to the uncertainty on the A_2 values.

F. γ-transitions in the decay of ^{33}Ar

To obtain a good calibration of the particle detectors several runs with ^{33}Ar were made during the experiment. The γ spectrum from these, i.e., in the decay of ^{33}Ar, can be seen in Fig. 14. The peak marked with numbers corresponds to transitions in the β-daughter ^{33}Cl, the ones marked with Roman numbers to transitions in the β-granddaughter ^{33}S and the one marked by a * to a transition in the β-proton daughter ^{32}S. A, B, C, and D are peaks from annihilation, pileup, and γ-transitions from decays of ^{40}K and ^{18}N, respectively. The assignment is supported by the half-life found for the peaks. The relative intensities of the γ lines observed in the decay of ^{33}Ar are given in Table IV. They are compared to results from three different experiments [34–36]. The line at 4734(3) keV from the transition between the IAS in ^{33}Cl and the first excited state in ^{33}Cl has not previously been observed in the decay of ^{33}Ar.

IV. SUMMARY

An improved half-life of ^{31}Ar of 15.1(3) ms has been determined. For the first time a spectroscopic analysis of

the decay mode of β-delayed three-proton emission has been presented, showing that in the case of ^{31}Ar roughly half of the $3p$ decays stem from the IAS in ^{31}Cl, while the rest stem from higher-lying levels. It is shown that the $3p$ emission is mainly sequential through the lowest levels above the proton threshold in ^{29}P, but a component of simultaneous emission cannot be excluded.

A quantitative analysis of $\beta 2p\gamma$ events has been performed and used to search for γ transitions from excited states in ^{29}P. Only γ rays from the two lowest excited states in ^{29}P could be clearly identified.

Analysis of all identified decay channels of the IAS including the $\beta 3p$ decay and contributions from decays to higher-lying states in ^{30}S than previously observed has led to an improved determination of the Fermi strength. The total measured branching ratio to the IAS is 3.60(44)%, which is lower than the theoretical value of 4.24(43)%, but the discrepancy is less than one standard deviation. This leaves room for contributions from decays to excited states in ^{29}P (above 1.96 MeV) and for a possible γ-decay channel of the IAS in ^{31}Cl.

A new method to determine the spin of low-lying levels in ^{30}S is presented. It uses angular correlations between the two protons in the $\beta 2p$ decay passing through the level of interest. Because the spin of the populated levels in ^{31}Cl is not known an ensemble of states in ^{31}Cl is used. The method is used for the level at 5.2 MeV, which is found to be either a 3^+ or 4^+ level, with the data favoring the 3^+. In previous studies this level has been suggested to be a 0^+ level [12] based on a comparison with the mirror nucleus, or as a 3^+ level based on its γ decay [29]. It is currently not known if there might be two levels around this energy, but we can conclude that a 3^+ level at 5.227(3) MeV is populated in the decay of ^{31}Ar. We see no indications that this peak may consist of two separate contributions in the present data.

Finally, the γ transitions in the decay of ^{33}Ar are measured and their relative intensities are given and compared to previous measurements. A new γ line from the decay of the IAS is found at 4734(3) keV.

ACKNOWLEDGMENTS

We thank Marek Pfützner for helpful discussion and input on the analysis of the $\beta 3p$-decay of ^{31}Ar. This work was supported by the European Union Seventh Framework through ENSAR (Contract No. 262010). This work was partly supported by the Spanish Funding Agency under Projects No. FPA2009-07387, No. FPA2010-17142, and No. AIC-D-2011-0684, by the French ANR (Contract No. ANR-06-BLAN-0320), and by Région Aquitaine. A.S. acknowledges support from the Jenny and Antti Wihuri Foundation.

[1] M. Pfützner *et al.*, Rev. Mod. Phys. **84**, 567 (2012).
[2] M. Borge *et al.*, Nucl. Phys. A **515**, 21 (1990).
[3] V. Borrel *et al.*, Nucl. Phys. A **473**, 331 (1987).
[4] L. Axelsson *et al.*, Nucl. Phys. A **628**, 345 (1998).
[5] H. O. U. Fynbo *et al.*, Nucl. Phys. A **677**, 38 (2000).
[6] B. A. Brown, Phys. Rev. Lett. **65**, 2753 (1990).
[7] K. Miernik *et al.*, Phys. Rev. C **76**, 041304 (2007).
[8] M. Pomorski *et al.*, Phys. Rev. C **83**, 014306 (2011).
[9] L. Audirac *et al.*, Eur. Phys. J. A **48**, 179 (2012).
[10] M. Pfützner *et al.*, GSI-SR2012-PHN-ENNA-EXP-17, GSI Report 2013-1 (2012).
[11] G. T. Koldste *et al.*, Phys. Rev. C **87**, 055808 (2013).
[12] K. Setoodehnia *et al.*, Phys. Rev. C **87**, 065801 (2013).
[13] G. T. Koldste *et al.* [Phys. Lett. B (to be published)] (2014), arXiv:1404.2143 [nucl-ex].
[14] E. Kugler, Hyperfine Interact. **129**, 23 (2000).
[15] L. Penescu *et al.*, Rev. Sci. Instrum. **81**, 02A906 (2010).
[16] I. Matea *et al.*, Nucl. Instrum. Methods Phys. Res., Sect. A **607**, 576 (2009).
[17] N. Warr *et al.*, Eur. Phys. J. A **49**, 40 (2013).
[18] K. Debertin and R. G. Helmer, *Gamma- and X-ray Spectrometry with Semiconductor Detectors* (North-Holland, Amsterdam, 1988).
[19] J. G. Johansen *et al.*, Phys. Rev. C **88**, 044619 (2013).
[20] D. C. Radford, Nucl. Instrum. Methods Phys. Res., Sect. A **361**, 297 (1995).
[21] L. Axelsson *et al.*, Nucl. Phys. A **634**, 475 (1998).
[22] D. Bazin *et al.*, Phys. Rev. C **45**, 69 (1992).
[23] H. O. U. Fynbo *et al.* (the ISOLDE Collaboration), Phys. Rev. C **59**, 2275 (1999).
[24] M. S. Basunia, Nucl. Data Sheets **113**, 909 (2012).
[25] Y. H. Lam *et al.*, At. Data Nucl. Data Tables **99**, 680 (2013).
[26] M. Bhattacharya *et al.*, Phys. Rev. C **77**, 065503 (2008).
[27] M. Wang *et al.*, Chin. Phys. C **36**, 1603 (2012).
[28] A. Saastamoinen, Ph.D. thesis, University of Jyväskylä, 2011.
[29] G. Lotay *et al.*, Phys. Rev. C **86**, 042801 (2012).
[30] S. Almaraz-Calderon *et al.*, Phys. Rev. C **86**, 065805 (2012).
[31] W. A. Richter and B. A. Brown, Phys. Rev. C **87**, 065803 (2013).
[32] L. C. Biedenharn and M. E. Rose, Rev. Mod. Phys. **25**, 729 (1953).
[33] R. B. D'Agostino and M. A. Stephens, *Goodness-of-Fit Techniques* (Dekker, New York, 1986).
[34] N. Adimi *et al.*, Phys. Rev. C **81**, 024311 (2010).
[35] M. J. G. Borge *et al.*, Phys. Scr. **36**, 218 (1987).
[36] H. S. Wilson, R. W. Kavanagh, and F. M. Mann, Phys. Rev. C **22**, 1696 (1980).